Polarization observations and results of the 1998 February 26th solar corona

J.-R. Gabryl, P. Cugnon and F. Clette

Observatoire Royal de Belgique
Belgium

Received: November 25, 1998

Abstract. In the frame of the long-term study program of the solar corona, we have organized an expedition in Curacao (Dutch Antillas) to observe the total solar eclipse of February 26th, 1998. As the totality duration was quite short, we had to improve again the CCD experiment layout in order to record a sample of images as wide as possible in both polarization and brightness ranges. This was made possible by the acquisition of a new PC with fast hard disc and data transfer port. We managed then to record 7 series of different exposures, each containing polarization measurements of 24 images (thus 8 times oversampled). The data processing led to accurate brightness and polarization maps as well as electron density models. The shape of the corona is highly flattened with large polar holes filled by numerous wide plumes. Large streamers are also observed and are essentially aligned along the solar equatorial plane. Moreover, the polarization indicates that these structures are located in the vicinity of the plane of the sky. Unfortunately, the unusually high sky brightness hid the faintest coronal structures and limited the visibility up to 3 solar radii implying a similar limitation in our modelling. We present here these results and give a brief comparison with our previous eclipse observation.

Key words: eclipses – whitelight corona – electron density

1. Eclipses observation

One way to deduce the electron density distribution in the solar corona is to perform white light polarized observations during total solar eclipses. These observations provide good brightness and polarization data as long as the sky transparency remains constant during totality. Moreover, we have stated in a previous paper dealing with 1994 eclipse observation (Gabryl and Cugnon, 1997) that increasing the polarization sampling does not only improve the observations accuracy but also allows to correct for sudden variations of sky transparency. In order to reach this purpose, we chose a new portable PC (Dolch PAC586) allowing high speed transfers between memory and hard disk and a new DC motor to speed up the polarizer rotation.

As a result, during the February 26th, 1998, we managed to record 168 images (744×580 pixels, $11'' \times 11.5''$ per pixel): 7 groups of different relative

Contrib. Astron. Obs. Skalnaté Pleso **28**, (1998), 216 – 223.

exposures containing 24 polarized images each. The polarization is then 8 times oversampled and the intensity dynamic is ranging from 1 to 2000. Furthermore, the meteorological conditions during the totality at our site (Watamula, Curacao, at a few meters above the sea level) were excellent even though an hour before the second contact some clouds were still covering the solar disc.

2. Data processing

The first step we performed was to realign all images on the solar disc centre. We used an intercorrelation algorithm to determine the Moon disc centre for each image and computed tables of the Moon motion relative to the Sun centered frame. The images were then corrected for the average dark frame and flat-fielded. Finally, each pixel value was corrected for non linearities of the camera response curve.

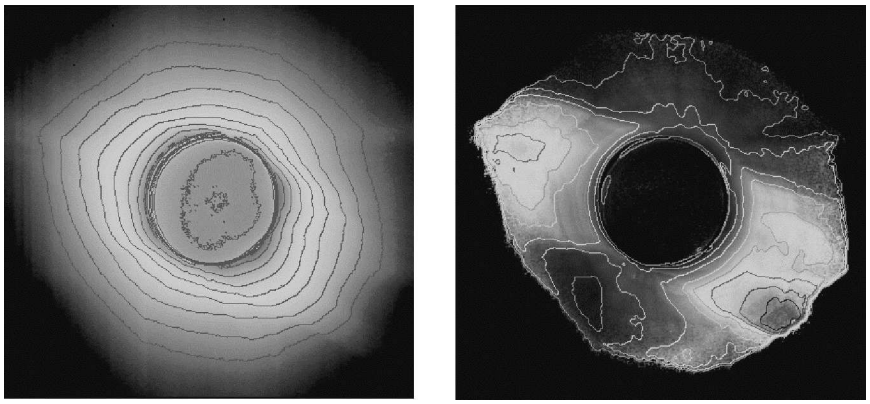

Figure 1. February 26th, 1998 solar corona. The total intensity, on the left, is represented in a logarithmic scale. The outer isophote is equal to $4 \times 10^{-9} B_{\odot}$ and the factor between two successive steps is 2. The polarization p_{K+F} is on the right. The outermost curve is equal to 15% of polarization and the step between two successive curves is 5%.

We calculated linear Stoke's parametres (named X, Y and I) for each group of 24 images using a least squares method, where 'I' stands for the intensity. Combining the parametres requires first to determine the constant intensity ratios between successive groups of different relative exposure. One exposure group is chosen to be the intensity scale reference. The intensity ratio between each of the other series and the reference serie is deduced sucessive step by successive step. All rescaled Stoke's parametres were then locally averaged following a statistical criterion. The absolute intensity scaling was finally performed using calibration measurements of the Sun disc centre brightness using the same optics equipped with a supplementary neutral density filter ND5. Saito's tables of the F corona brightness for a polar hole and the ratio of this brightness to

the total brightness were used to check the validity of our calibration. Thanks to this check, we were able to determine an averaged sky brightness which was unfortunately high enough to mask the typical polar brightnesses beyond 2.5 $R_\odot$ and the streamer brightnesses beyond 3.1 $R_\odot$. After removing a constant sky background, we got the calibrated total brightness of the corona (Figure 1) and the polarized brightness from which we calculated the polarization (Figure 1).

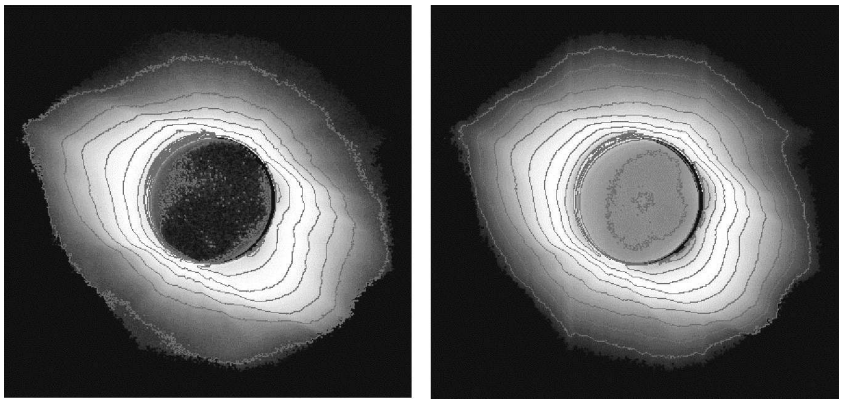

Figure 2. From left to right, February 26th, 1998 polarized and K corona brightnesses represented in a logarithmic scale. The outer isophotes respectively correspond to $2 \times 10^{-9} B_\odot$ and $4 \times 10^{-9} B_\odot$. The factor between two successive isophotes is 2.

In these pictures, the vertical direction is that of the celestial poles with the North at the top, so that the North of the Sun rotation axis is tilted by 20.7° Westward. The global corona structure appears flattened much more like a minimum type corona than an intermediate type corona as we expected. It is noticeable that the maximum of polarization (54%) occurs at 2.5 $R_\odot$ in the WSW streamer (at PA=230°). As a consequence, this streamer appears to be close to the plane of the sky. However, considering observed average values, the maximum position may appear too distant. In fact, the constant sky brightness we substracted could have been too high for that region, although no substraction at all would have led to a maximum at 2.2 $R_\odot$. We then think that our conclusion concerning the streamer configuration still holds.

3. Modelling the electron density distribution

It is well known (Gabryl and Cugnon, 1997; Clette, 1997) that van de Hulst's integral equations (Equations 1, 2) which characterizethe elctron density problem do not allow a full 3-D reconstruction from eclipse observations:

$$K_t(x, \Psi) = C \int_x^\infty N_e A(r) \frac{r dr}{\sqrt{r^2 - x^2}} \tag{1}$$

$$(K_t - K_r)(x, \Psi) = C \int_x^{\infty} N_e(A(r) - B(r)) \frac{x^2 dr}{r\sqrt{r^2 - x^2}} \quad (2)$$

It is then necessary to introduce a supplementary hypothesis to invert these equations. Our point consist in assuming an axisymmetric electron density distribution of which the latitude dependency is described by an expansion into Legendre polynomials. At each polynomial, a radial function in 1/r takes into account the density radial decrease (Equation 3).

$$N_e(r, \varphi) = \sum_{n=0}^{N_{max}} P_n(\sin \varphi) \sum_{i=1}^{I_{max}(n)} \frac{a_{i,n}}{r^{b_{i,n}}} \quad (3)$$

A powerful feature of this model is to allow the choice of the symmetry axis and the level of complexity (i.e. the number of Legendre polynomials and the number of radial terms). Furthermore, this expression (Equation 3) gives analytical solutions to the integral equations. So, the determination of the parametres, i.e. coefficients $a_{i,n}$ and exponents $b_{i,n}$, is based on a least squares method applied in two successive steps. The first step takes into account the angular variations of the data and produces radial functions on which the parametres are fitted at the second step. In theory, the modelling implies a mixing of East and West half data, considering that the symmetry axis projected on the plane of the sky separates the corona in two half planes. However, only the electrons located in the vicinity of the plane of the sky strongly contribute to the integration along the lines of sight, so that we practically may calculate two separate models, one per half data. Moreover, our experience tells us that a good 2-D decription is obtained with a polynomial expansion up to the order 6 or 7 and two or three radial terms per polynomial.

The following pictures represent the data prior to the modelling, i.e. the polarized brightness and the K corona brightness (Figure 2) which has been calculated by removing Saito F corona from our calibrated total brightness. Then, we plotted a 2-D model (Figure 3) expansed up to the seventh polynomial order with the Sun rotation axis as the symmetry axis. As one can see, the highest densities are located at the base of the opposite large streamers and barely reach $10^{14} e/m^3$.

4. Comparison with 1991 and 1994 results

As our study is dealing with the long term evolution of the corona, we compared this last model with those calculated from our 1991 and 1994 observations. The Figure 4 shows the three reconstructions together. The scaling is the same in the three pictures and the vertical direction is that of the projected rotation axis of the Sun with the North at the top. Up to now, only the 1991 corona model exhibits structures with high densities at high latitudes. In fact, against

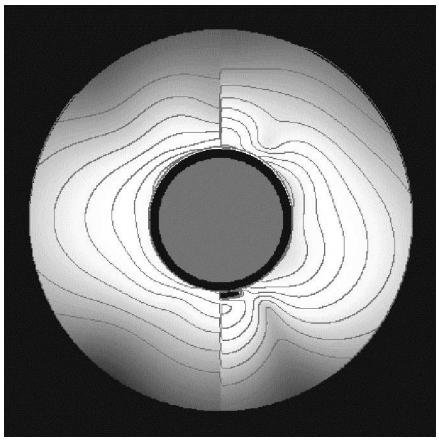

Figure 3. February 26th, 1998 electron density reconstruction expanded up to the 7th Legendre polynomial. The symmetry axis is the Sun rotation axis. The densities are plotted in a logarithmic scale. The outermost curve is equal to $2 \times 10^{11} e/m^3$ and the factor between two successive curves is 2.

our own expectations, the 1998 density model is closer to the minimum type reconstruction obtained in 1994, although the solar activity is in the ascent phase for two years. However, even if the 1998 inner densities near the equator are just lower or equal to the 1994 inner densities, the radial gradients are much smoother in the 1998 model, so that 1998 equatorial values are of the same order of magnitude than the 1991 streamer values at large distances. In that sense, the 1998 corona could be an intermediate type corona.

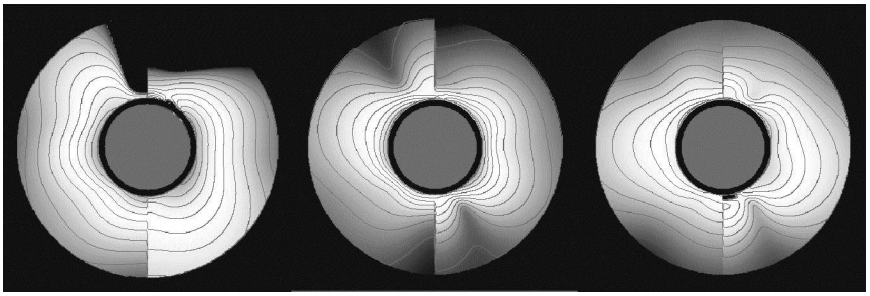

Figure 4. Comparison between 1991 (left), 1994 (centre), and 1998 (right) density reconstructions. Once again, the logarithmic scale is chosen so that the factor between two successive curves is 2. The outermost density curves respectively correspond to $1 \times 10^{11} e/m^3$, $1 \times 10^{11} e/m^3$ and $2 \times 10^{11} e/m^3$.

Radial density profiles taken along typical structures from the different eclipse results lead us to the same conclusion (Figures 5,6,7). These plots also reveal a kind of density regimes: considering that the measured extreme radial profiles (streamer and hole profiles) limit a density area, the 1991 density area

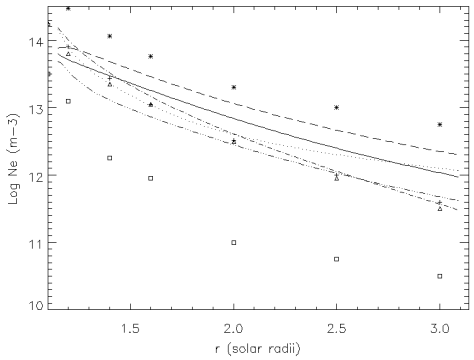

Figure 5. Electron density radial profiles extracted from the 1991 density reconstruction at different latitudes. The dotted and dash dot dot profiles are relative to polar regions while the continuous profile is relative to a typical streamer. Discrete symbols are Koutchmy's tabulated values for a polar hole (□), a streamer (∗), the equatorial region during maximum activity (+) and minimum activity (△).

fills the band between 'equatorial' and 'streamer' tabulated profiles, while the 1994 density area fills the band between 'polar' and 'equatorial' profiles, and the 1998 density area is approximately centered on the 'equatorial' tabulated profiles.

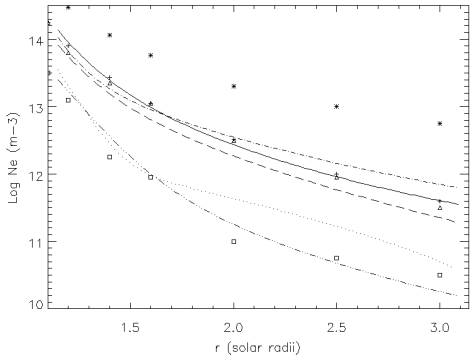

Figure 6. Electron density radial profiles extracted from the 1994 density reconstruction at different latitudes. The dotted and dash dot dot profiles are relative to polar regions while the continuous profile is relative to a typical streamer. Discrete symbols are Koutchmy's tabulated values for a polar hole (□), a streamer (∗), the equatorial region during maximum activity (+) and minimum activity (△).

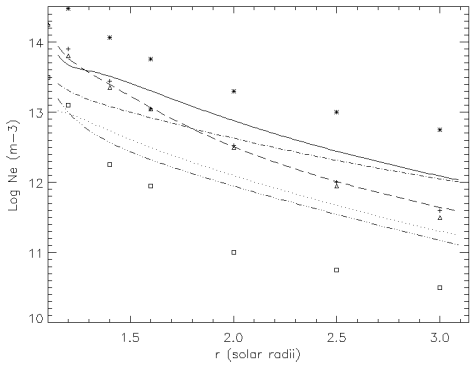

Figure 7. Electron density radial profiles extracted from the 1998 density reconstruction at different latitudes. The dotted and dash dot dot profiles are relative to polar regions while the continuous profile is relative to a typical streamer. Discrete symbols are Koutchmy's tabulated values for a polar hole ($\Box$), a streamer ($*$), the equatorial region during maximum activity ($+$) and minimum activity ($\triangle$).

5. Conclusions

The large scale electron density distribution model we have developed has proved to be reliable: the calculated densities from our different eclipse observations are fully compatible with the typical values. Moreover, thanks to the long-term run, it allows to study the density variations with respect to the solar cycle. So, the transition between the minimum corona and the maximum corona seems to be characterized first by an increase of the electron density in the outer corona, so that the observed radial gradients are smoother. In the context of an isothermal hydrostatic corona (Badalyan, 1986; Gabryl and Cugnon, 1997), this means that the temperature is increasing. In order to go on studying this evolution, a fruitful observation of the August 11th, 1999 total solar eclipse is important as LASCO C1 is not available for the white-light bandwidth. That's why we plan to multiply our CCD experiment along the totality band in Europe (Cugnon et al., these issue).

References

Badalyan, O. G.: 1986, *Astron. Astrophys.* **169**, 305

Clette, F.: 1997, in *Theoretical and Observational Problems Related to Solar Eclipses*, eds.: Z. Mouradian and M. Stavinschi, Kluwer Academic Publishers, Dordrecht, 103

Gabryl, J.-R. and Cugnon, P.: 1997, in *Theoretical and Observational Problems Related to Solar Eclipses*, eds.: Z. Mouradian and M. Stavinschi, Kluwer Academic Publishers, Dordrecht, 73

Guhathakurta, M. et al.: 1997, in *The Corona and Solar Wind Near Minimum Activity*, ed.: Wilson A., ESA Publications Division and ESTEC, Noordwijk, 421
Koutchmy, S.: 1992, *Prepublication of the Institut d'Astrophysique de Paris* **404**, 23
Romoli, M. et al.: 1997, in *The Corona and Solar Wind Near Minimum Activity*, ed.: Wilson A., ESA Publications Division and ESTEC, Noordwijk, 633
Saito, K.: 1970, *Ann. Tokyo Astron. Obs., Second Ser.* **12**, 53

Discussion

Question (S. Koutchmy): *On your last graph you presented the distribution of densities over a cross-section of the corona. Polar regions show enhanced densities and edge of polar region show a decreased densities which are the opposite of what we expect for a coronal hole. Besides an axisymmetry, what additional assumption are made to deduce a such distribution?*

Answer (P. Cugnon): There is, in fact, no other assumption than the axisymmetric assumption. The problem may arise from a defect in calibration which effects much more the regions of weak brightnesses. This point will be more investigated.

Question (I. Vince): *What kind of CCD camera did you use for polarimetric observation of the corona? Was it cooled?*

Answer (P. Cugnon): It was a PULNIX CCD video camera 744x580 pixels - the pixel clock allows a synchrone digital acquisition (8 bits). Cooled by Peltier effect.